



This is a repository copy of *Virtual Signal Injection-Based Direct Flux Vector Control of IPMSM Drives*.

White Rose Research Online URL for this paper:
<http://eprints.whiterose.ac.uk/105456/>

Version: Accepted Version

Article:

Sun, T. orcid.org/0000-0002-5518-0315, Wang, J. orcid.org/0000-0003-4870-3744 and Koc, M. orcid.org/0000-0003-1465-1878 (2016) Virtual Signal Injection-Based Direct Flux Vector Control of IPMSM Drives. *IEEE Transactions on Industrial Electronics*, 63 (8). pp. 4773-4782. ISSN 0278-0046

<https://doi.org/10.1109/TIE.2016.2548978>

Reuse

Unless indicated otherwise, fulltext items are protected by copyright with all rights reserved. The copyright exception in section 29 of the Copyright, Designs and Patents Act 1988 allows the making of a single copy solely for the purpose of non-commercial research or private study within the limits of fair dealing. The publisher or other rights-holder may allow further reproduction and re-use of this version - refer to the White Rose Research Online record for this item. Where records identify the publisher as the copyright holder, users can verify any specific terms of use on the publisher's website.

Takedown

If you consider content in White Rose Research Online to be in breach of UK law, please notify us by emailing eprints@whiterose.ac.uk including the URL of the record and the reason for the withdrawal request.



eprints@whiterose.ac.uk
<https://eprints.whiterose.ac.uk/>

Virtual Signal Injection Based Direct Flux Vector Control of IPMSM Drives

Tianfu Sun, Student Member, IEEE, Jiabin Wang, Senior Member, IEEE, and Mikail Koc, Student Member, IEEE

Abstract— This paper describes a novel virtual signal injection (VSI) based direct flux vector control (DFVC) for maximum torque per ampere (MTPA) operation of interior permanent magnet synchronous machine (IPMSM) in constant torque region. The proposed method virtually injects a small high frequency current angle signal for tracking the optimal flux amplitude of MTPA operation. This control scheme is not affected by the accuracy of flux observer and independent of machine parameters in tracking the MTPA points and will not cause additional iron loss, copper loss and torque ripple as a result of real signal injection. Moreover, by employing a band-pass filter with a narrow frequency range the proposed control scheme is also robust to current and voltage harmonics, and load torque disturbances. The proposed method is verified by simulations and experiments under various operating conditions on a prototype IPMSM drive system.

Index Terms— Direct flux vector control, interior permanent magnet synchronous machine (IPMSM) drives, maximum torque per ampere (MTPA), signal injection, virtual signal injection (VSI).

I. INTRODUCTION

INTERIOR permanent magnet synchronous motors (IPMSM) have many attractive advantages in high performance drive applications due to their high power density, high efficiency [1], and wide constant power speed range [2]. To control the IPMSM, either field oriented control (FOC) in the rotor synchronous reference (d-q) frame or direct torque control (DTC) [3]–[6] and direct flux vector control (DFVC) [7]–[9] in the flux and torque (f-t) reference frame can be adopted. Compared with d-q frame based control schemes, the f-t frame based control schemes not only can manage motor voltage in field weakening region without look-up tables of current or flux references [10] but also has better performance in field weakening [11], fast torque response [12], and higher torque control accuracy.

In order to operate IPMSM in constant torque region effectively, the maximum torque per ampere (MTPA) control is necessary. In literature, the MTPA strategies for d-q frame

based control scheme are well studied. However, the MTPA control strategies for f-t frame based control schemes are less reported. Different from d-q frame based MTPA control schemes, the performances of f-t frame based MTPA control schemes are not only dependent on the accuracy of commands generated by the MTPA control schemes, but also dependent on the accuracy of flux observer.

Currently, the MTPA operations for f-t frame based control schemes are similar to the d-q frame based schemes. However, instead of controlling d-axis current or current angle in d-q frame based MTPA control, the MTPA operation for f-t frame based control schemes is mainly achieved by controlling the reference flux amplitude. The reference flux amplitude for MTPA operation can either be calculated based on mathematical model [13] or generated from pre-defined look-up tables which are obtained from numerical machine model or experiments [8]. However, in real applications, the parameters of IPMSM are highly nonlinear and uncertain [14]. Therefore, it is almost impossible to obtain accurate reference flux amplitude according to predefined look-up tables or mathematical model.

Recently, new methods base on the principle of extremum seeking control (ESC) [15]–[17] for tracking the MTPA points by injecting high-frequency current signals into machines have been reported. In [18], a signal injection based MTPA point tracking scheme in the f-t frame was proposed. In order to avoid the residual torque harmonic at the frequency of the injected signal, a random signal was injected into reference flux amplitude instead of the pure sinusoidal signal injection. And the MTPA points were tracked based on the fact that the current amplitude variation with respect to injected reference flux amplitude perturbation at MTPA points is zero [18]. However, this method may induce additional iron/copper loss as well as additional torque ripple as a result of the injected signal. Moreover similar to other f-t frame based control techniques, this method did not consider the influence of flux observer error on MTPA operations.

In this paper, a f-t frame based control scheme employing the newly reported virtual signal injection (VSI) [19]–[21] in d-q frame is proposed for the MTPA operation of IPMSM drives in constant torque region. Without loss of generality, the direct flux vector control scheme is selected to demonstrate the proposed control scheme. The proposed control scheme retains the advantages of the f-t frame based control schemes but eliminates the problems associated with real signal injection. Moreover, the proposed control scheme is robust to flux observer error and motor parameters inaccuracy in tracking

Manuscript received July 19, 2015; revised October 18, 2015, December 11, 2015 and January 30, 2016; accepted March 10, 2016.

T. Sun, J. Wang and M. Koc are with the Department of Electronic and Electrical Engineering, The University of Sheffield, Mappin Street, Sheffield S1 3JD, United Kingdom (e-mail: tianfu.sun@foxmail.com, j.b.wang@sheffield.ac.uk, mikaelkoc@gmail.com).

MTPA points.

II. PRINCIPLE OF PROPOSED CONTROL SCHEME

Control schemes of IPMSM drives can be based on the flux and torque (f-t) reference frame whose relationship with respect to the classic (d-q) frame is illustrated in Fig. 1. The f-axis is aligned with the stator flux vector while the t-axis leads the f-axis by 90 degrees. Both the d-q frame and f-t frame rotate in synchronism with the rotor and their angular displacements with respect to the stationary α -axis are θ_e and $\theta_e + \delta$, respectively.

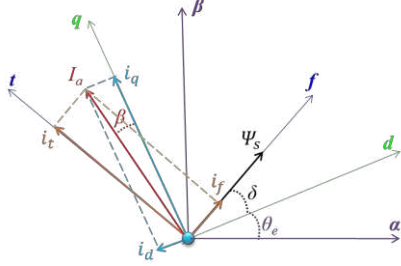


Fig. 1. α - β reference frame, f-t reference frame and d-q reference frame.

A. Mathematical model of IPMSM

The mathematical model of an IPMSM in the d-q reference frame can be expressed in (1) to (3) when high order harmonics are neglected. L_d and L_q in (1) to (3) are the d- and q-axis inductances, v_d and v_q are the d- and q-axis voltages, and i_d and i_q are the d- and q-axis currents, respectively. Ψ_m is the flux linkage due to permanent magnets, R is the stator resistance, p is the number of pole pairs, T_e is the electromagnetic torque and ω_m is rotor angular speed.

$$v_q = L_q \frac{di_q}{dt} + Ri_q + p\omega_m L_d i_d + p\omega_m \Psi_m \quad (1)$$

$$v_d = L_d \frac{di_d}{dt} + Ri_d - p\omega_m L_q i_q \quad (2)$$

$$T_e = \frac{3p}{2} [\Psi_m i_q + (L_d - L_q) i_d i_q] \quad (3)$$

In the field oriented control scheme, for a given torque demand, there is a unique set of optimal d- and q-axis currents for MTPA operation, and the optimal d- and q-axis currents are controlled by two current feedback loops.

To achieve the direct control of stator flux and torque, the mathematical model of an IPMSM can be expressed in the f-t reference frame in (4) to (8) [22], where v_f and v_t are the f- and t-axis voltages, and i_f and i_t are the f- and t-axis currents, respectively. Ψ_s is the stator flux vector amplitude, and δ is the angle of the stator flux vector with respect to the d-axis. I_{lim} is the current limit.

$$v_f = Ri_f + \frac{d\Psi_s}{dt} \quad (4)$$

$$v_t = Ri_t + \Psi_s \left(p\omega_m + \frac{d\delta}{dt} \right) \quad (5)$$

$$T_e = \frac{3}{2} p \Psi_s i_t \quad (6)$$

$$\sqrt{I_{lim}^2 - i_f^2} \geq i_t \quad (7)$$

$$\frac{3}{2} p \Psi_s \sqrt{I_{lim}^2 - i_f^2} \geq T_e \quad (8)$$

An f-t frame based control scheme can be formulated by controlling Ψ_s and i_t when the stator flux is estimated by a flux observer. The reference flux amplitude for MTPA operations may be generated from a numerical model of the IPMSM and the data is stored in the controller in a look-up table. However, the reference flux amplitude may deviate from the MTPA value when the flux map of the actual machine differs from the model because of temperature variation and other modeling errors. Although this problem may partly be circumvented by the signal injection control proposed in [18], the flux observer error may bring additional control error which affects MTPA operations. Further, in the field oriented control, a deviation of d-axis current from its true MTPA point only affects the second term in (3). Hence the resulting torque control error is relatively small. With the f-t frame based control, errors in Ψ_s , whether it is generated from the reference or from the observer, will cause larger torque deviation as is evident from (6). Therefore, the MTPA operation in the f-t frame is more sensitive to flux errors and the accuracy of MTPA control is more difficult to be guaranteed.

B. Relationship between Ψ_{sMTPA} and β_{MTPA}

For a given current amplitude, I_a , in (9), the relationship between T_e and the current angle, β defined in (10), can be expressed in (11).

$$I_a = \sqrt{i_d^2 + i_q^2} \quad (9)$$

$$\beta = \arccos\left(\frac{i_q}{I_a}\right) \quad (10)$$

$$T_e = \frac{3p}{2} \left[\Psi_m I_a \cos(\beta) - \frac{1}{2} (L_d - L_q) I_a^2 \sin(2\beta) \right] \quad (11)$$

The optimal current angle, β_{MTPA} , for MTPA operation is obtained when $\partial T_e / \partial \beta$ is equal to zero. The MTPA stator flux amplitude, Ψ_{sMTPA} , for given current amplitude is expressed in (12).

$$\Psi_{sMTPA} = \sqrt{[\Psi_m - I_a L_d \sin(\beta_{MTPA})]^2 + [I_a L_q \cos(\beta_{MTPA})]^2} \quad (12)$$

Meanwhile, under MTPA operation, $\partial T_e / \partial \beta = 0$, according to (11), the relationship between β_{MTPA} and I_a can be expressed by (13).

$$I_a = \frac{\Psi_m \sin(\beta_{MTPA})}{(L_q - L_d)[1 - 2\sin^2(\beta_{MTPA})]} \quad (13)$$

Substitute (13) into (12), the relationship between β_{MTPA} and Ψ_{sMTPA} can be expressed by (14).

$$\Psi_{sMTPA} = \sqrt{a^2 + b} \quad (14)$$

where,

$$a = \Psi_m - \frac{\Psi_m L_d \sin^2(\beta_{MTPA})}{(L_d - L_q)[2\sin^2(\beta_{MTPA}) - 1]} \quad (15)$$

$$b = \frac{\Psi_m^2 L_q^2 \cos^2(\beta_{MTPA}) \sin^2(\beta_{MTPA})}{(L_d - L_q)^2 [2\sin^2(\beta_{MTPA}) - 1]^2} \quad (16)$$

It follows from (14) that for given I_a there is unique relationship between Ψ_{sMTPA} and β_{MTPA} . Therefore, Ψ_{sMTPA} can be obtained through adjusting the current angle β to its optimal value and vice versa.

By way of example, Figs. 2 (a) and (b) show the variation of β and the variation of T_e with the stator flux amplitude, respectively, for a prototype IPMSM whose specification is given in Table I.

As it is shown in Fig. 2 (b), when the stator flux amplitude increases, T_e initially increases and reaches a maximum before decreases. This maximum condition corresponds to MTPA operation. It is also evident from Fig. 2 (a), the Ψ_{SMTPA} can be found by adjusting β such that $\partial T_e / \partial \beta = 0$.

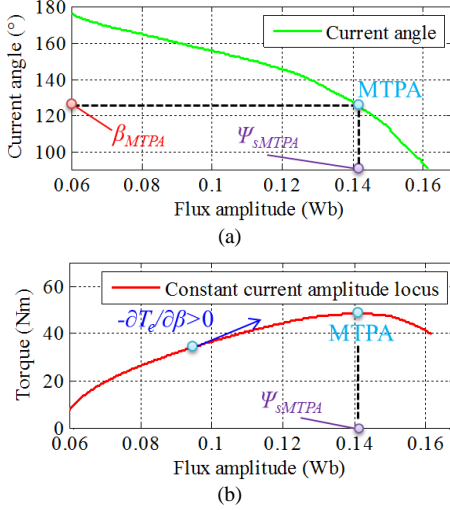


Fig. 2. (a) Relationship between flux amplitude and current angle. (b) Relationship between flux amplitude and resultant torque.

From Figs. 2 (a) and (b), $\partial T_e / \partial \beta$ will be negative when the stator flux amplitude is smaller than Ψ_{SMTPA} , and vice versa. This characteristic of $\partial T_e / \partial \beta$ is utilized by the proposed control scheme to track the MTPA point.

C. Virtual signal injection

The concept of the virtual signal injection (VSI) is briefly outlined and more details can be found in [19], [21]. Since iron loss has negligible influence on MTPA operation [19], the electromagnetic torque of an IPMSM can be expressed in (17). Where v_d^* and v_q^* are the reference d- and q-axis voltages with inverter voltage drop compensation, respectively.

$$T_e = \frac{3}{2} \left[\frac{(v_q^* - Ri_q)}{\omega_m} + \frac{(v_d^* - Ri_d)}{i_q \omega_m} \right] i_q \quad (17)$$

If a small high frequency sinusoidal signal $\Delta\beta = A \sin(\omega_h t)$ is mathematically injected to the stator current angle, β , the resultant d- and q-axis currents with the high frequency component can be expressed in (18) and (19). ω_h is the angular frequency of the injected signal.

$$i_d^h = -I_a \sin(\beta + \Delta\beta) \quad (18)$$

$$i_q^h = I_a \cos(\beta + \Delta\beta) \quad (19)$$

Substitute (18) and (19) into (17), the fluctuation of T_e with respect to $\Delta\beta$ can be calculated by (20).

$$T_e^h(\beta + A \sin(\omega_h t)) = \frac{3}{2} \left[\frac{(v_q^* - Ri_q)}{\omega_m} + \frac{(v_d^* - Ri_d)}{i_q \omega_m} \right] i_d^h \quad (20)$$

Although (20) is obtained from a mathematical calculation, it is equivalent to the effect of a real signal injection since $(v_q^* - Ri_q) / \omega_m$ and $(v_d^* - Ri_d) / (i_q \omega_m)$ in (20) can be considered as

constants over the period of the injected high frequency signal as indicated in [19]. The torque fluctuation given by (20) as a result of the VSI forms the basis for extracting $\partial T_e / \partial \beta$ as described subsequently.

D. $\partial T_e / \partial \beta$ information extraction

Based on Taylor's series expansion, the left hand side of (20) can be expressed in (21).

$$T_e^h(\beta + A \sin(\omega_h t)) = T_e^h(\beta) + \frac{\partial T_e^h}{\partial \beta} A \sin(\omega_h t) + \frac{1}{2} \frac{\partial}{\partial \beta} \left(\frac{\partial T_e^h}{\partial \beta} \right) A^2 \sin^2(\omega_h t) + \dots \quad (21)$$

The first order term of (21) contains the information of $\partial T_e / \partial \beta$ and it can be extracted by a band-pass filter (BPF) whose center frequency is equal to ω_h . If the output of band-pass filter is further multiplied by $\sin(\omega_h t)$, the result can be expressed in (22).

$$m \frac{\partial T_e}{\partial \beta} A \sin^2(\omega_h t) = \frac{1}{2} mA \frac{\partial T_e}{\partial \beta} - \frac{\partial T_e}{\partial \beta} mA \cos(2\omega_h t) \quad (22)$$

m is the gain of the band-pass filter at ω_h . The first term of the right hand side of (22), which is proportional to $\partial T_e / \partial \beta$, can be extracted by a low-pass filter (LPF). In this way the information which is proportional to $\partial T_e / \partial \beta$ in (20) can be extracted by the signal processing. When the output of the signal processing unit is equal to zero, the MTPA operation can be inferred. Otherwise the information of $\partial T_e / \partial \beta$ can be utilized to adjust the stator flux amplitude reference until it reaches the optimal value. Details about this adjustment will be given in Section III.

The proposed virtual signal injection for tracking MTPA points is parameter independent and is robust to current and voltage harmonics which are always present in a real IPMSM drive. Moreover, the virtual signal injection does not cause undesirable torque ripple, nor incur additional iron/copper losses. It is worth noting that due to the inverter voltage drop, the reference d- and q-axis voltages may not equal to the actual d- and q-axis voltages applied to motor. The voltage drop can be compensated by inverter voltage drop compensation schemes [23]. Additionally, the inverter nonlinearity effects can be avoided by measuring the inverter output voltages directly. The measured voltages are filtered by low-pass filters and converted into d- and q-axis voltages. After the effect of the filters is compensated, the actual d- and q-axis voltages can be obtained. Therefore, T_e^h also can be evaluated from (20) when v_d^* , v_q^* in (20) are substituted by the measured d- and q-axis voltages. However, this needs additional hardware such as voltage sensors and low-pass filter circuits. In practical applications, since the virtual signal injection tracks MTPA points by detecting the sign of $\partial T_e / \partial \beta$ and the MTPA operation is robust in d-q frame, therefore, even without inverter voltage drop compensation, the influence of inverter voltage drop on the proposed control scheme is still small.

III. IMPLEMENTATION OF THE PROPOSED CONTROL SCHEME

In this section, the details for implementing the proposed control scheme are described. The proposed control scheme can be divided into two parts, as shown in Fig. 3. The first part is a conventional direct flux vector control scheme proposed in [8]

which is utilized to generate nominal reference flux linkage, Ψ_{main} , and reference t-axis current for MTPA operation with fast response. The second part of the proposed control scheme

is a compensation loop based on the VSI to correct the errors of the reference flux Ψ_{main} and the observed flux.

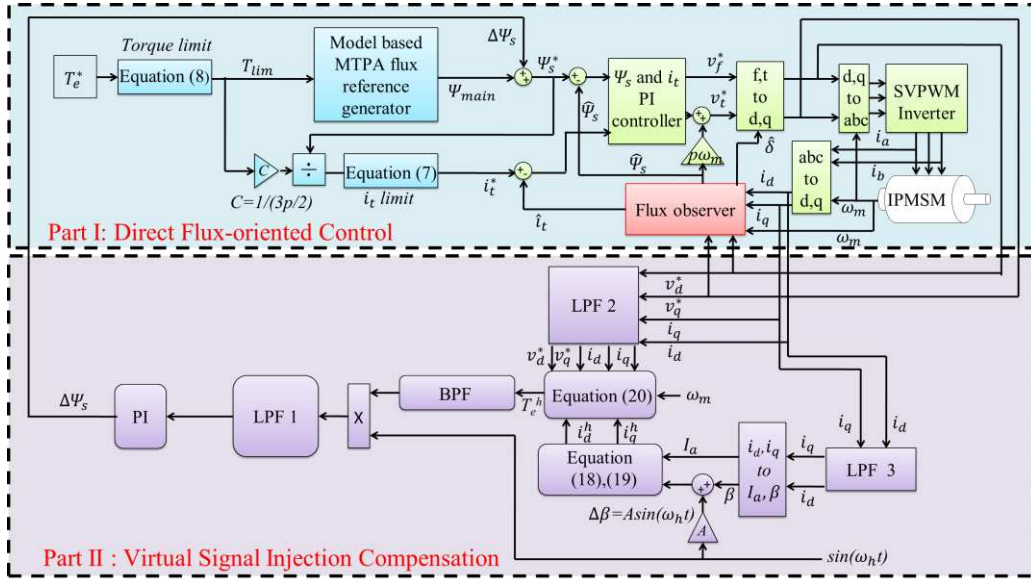


Fig. 3. Schematic of proposed control scheme.

A. Direct flux vector control

The direct flux vector control (DFVC) scheme [7]–[9] is adopted by the proposed control scheme as an example of the f-t frame based control scheme shown in Part I of Fig. 3. To ensure the IPMSM drive operates within the current and voltage limits, the reference torque, T_e^* , is limited by (8). A predefined look-up table is utilized to produce the nominal reference flux amplitude, Ψ_{main} . The input of the look-up table is the limited reference torque, T_{lim} , generated from (8). The look-up table is computed off-line from a high fidelity nonlinear IPMSM machine model based on FE analysis [24]. The t-axis reference current, i_t^* , is generated according to (6) and limited by (7). The observed flux amplitude and t-axis current are denoted by $\hat{\Psi}_s$ and \hat{i}_t respectively. As proposed in [7], the stator flux linkage is directly regulated by the f-axis voltage while the t-axis current is regulated by the t-axis voltage. More details for the DFVC can be found in [7].

However, due to machine parameters variation and uncertainty, the accuracy of Ψ_{main} generated from the look-up table cannot be guaranteed. Moreover, due to errors in the flux observer, $\hat{\Psi}_s$ and \hat{i}_t and the observed angle between the f-axis and the d-axis, $\hat{\delta}$, may not equal to their actual values, which will also affect the MTPA control performance significantly. In order to compensate these errors, an error compensation term $\Delta\Psi_s$ is needed.

B. Flux amplitude reference error compensation

The reference flux amplitude compensation term $\Delta\Psi_s$ is generated from Part II of Fig. 3 according to the VSI and $\partial T_e / \partial \beta$ information extraction described in Section II.

As shown in Part II of Fig. 3, the measured d- and q-axis currents are filtered by a low-pass filter denoted as LPF 3 to eliminate high order harmonics. The filtered d- and q-axis currents are transformed into the polar coordinate system by (9) and (10) to obtain β and I_a . The d- and q-axis current

perturbations with the injected high frequency signal are calculated from (18) and (19). The resultant torque variation T_e^h is obtained from (20) based on the output of (18) and (19), i_d^h , i_q^h , the filtered d- and q-axis reference voltages, the filtered d- and q-axis currents, and the measured rotor speed. In order to extract the first order term of (21), the torque perturbation T_e^h is filtered by a band-pass filter (BPF). The output of the BPF is further multiplied by $\sin(\omega_h t)$ before being fed to the low-pass filter denoted as LPF 1 to obtain the signal proportional to $\partial T_e / \partial \beta$.

The output of the LPF 1 is used by a PI controller to produce $\Delta\Psi_s$. The gains of the PI controller are negative since when the stator flux amplitude is smaller than Ψ_{sMTPA} as shown in Fig. 2 (b), $-\partial T_e / \partial \beta > 0$ and vice versa. Thus, the PI controller will adjust the reference flux amplitude, Ψ_s^* , such that when it is lower than Ψ_{sMTPA} , it will be increased, or otherwise decreased until $\partial T_e / \partial \beta = 0$, i.e., the MTPA point is reached. In this way, the error of Ψ_{main} is compensated by $\Delta\Psi_s$. Ψ_s^* is the combination of the Ψ_{main} and the $\Delta\Psi_s$.

It is worth noting that the voltages and currents in (20) are in d- and q-axis components, therefore, the VSI based feedback loop will not be affected by the inaccuracies in the observed quantities, such as f- and t-axis currents, flux amplitude and the angle $\hat{\delta}$. Therefore, although flux observer error may cause torque control error, the accuracy of the proposed control scheme in tracking MTPA operation of actual torque will not be affected. This property will be demonstrated by simulations and experiments in Section IV and Section V, respectively.

C. Flux observer

For the f-t reference frame based control, a flux observer is needed. In this paper, the conventional observer introduced in [25] is adopted. The block diagram of the flux observer is shown in Fig. 4. However, other kinds of observer are also possible for the proposed control scheme.

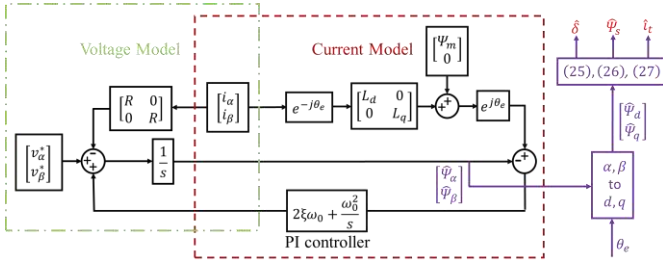


Fig. 4. Flux and torque observer.

The flux observer in Fig. 4 consists of a voltage model given in (23) and a current model given in (24), where $\hat{\Psi}_\alpha$ and $\hat{\Psi}_\beta$ are the observed α - and β -axis flux components. v_α^* and v_β^* are the α - and β -axis reference voltages, i_α and i_β are the measured α - and β -axis currents and θ_e is the rotor angular position.

$$\begin{bmatrix} \hat{\Psi}_\alpha \\ \hat{\Psi}_\beta \end{bmatrix} = \begin{bmatrix} \frac{1}{s} (v_\alpha^* - R i_\alpha) \\ \frac{1}{s} (v_\beta^* - R i_\beta) \end{bmatrix} \quad (23)$$

$$\begin{bmatrix} \hat{\Psi}_\alpha \\ \hat{\Psi}_\beta \end{bmatrix} = \begin{bmatrix} \cos\theta_e & -\sin\theta_e \\ \sin\theta_e & \cos\theta_e \end{bmatrix} \begin{bmatrix} L_d i_d + \Psi_m \\ L_q i_q \end{bmatrix} \quad (24)$$

The voltage model is parameter-independent except for the phase resistance. However, at high speed, the voltage drop across the resistance is relatively small, and the voltage model based observer is accurate at high speeds while its accuracy become poor at low speeds since inverter voltage drop is significant. The current model is more accurate at low speeds, but it is parameter dependent. The difference between the voltage model based observer and the current model based observer is used by a PI controller to achieve the best combination of the two. ξ and ω_0 of the PI controller in Fig. 4 are the damping ratio and crossover frequency, respectively, associated with the combination of the two outputs. The voltage model will be dominant above the predefined crossover frequency while the current model will be dominant below the crossover frequency [25].

The observed d- and q-axis fluxes, $\hat{\Psi}_d$ and $\hat{\Psi}_q$, can be obtained through $\hat{\Psi}_\alpha$, $\hat{\Psi}_\beta$ and θ_e , as shown in Fig. 1. The estimated angle between the f-axis and the d-axis, $\hat{\delta}$, can be calculated from (25):

$$\hat{\delta} = \tan^{-1} \frac{\hat{\Psi}_q}{\hat{\Psi}_d} \quad (25)$$

The observed flux amplitude $\hat{\Psi}_s$ can be calculated from (26):

$$\hat{\Psi}_s = \sqrt{\hat{\Psi}_d^2 + \hat{\Psi}_q^2} \quad (26)$$

The observed t-axis current, \hat{i}_t , can be generated from (27) with the measured d- and q-axis currents, i_d and i_q .

$$\hat{i}_t = i_q \cos \hat{\delta} - i_d \sin \hat{\delta} \quad (27)$$

IV. SIMULATION STUDIES

Simulations were performed based on a prototype IPMSM drive system. The motor specification is given in Table I and it is designed for distributed traction of a micro-size electric vehicle with peak power of 10 kW at base speed of 1350 r/min. The d- and q-axis inductances and the permanent magnet flux linkage of the machine are highly non-linear and vary

significantly with currents because of magnetic saturation. ξ and ω_0 in Fig. 4 are set to 0.707 and 50π rad/s, respectively. The crossover frequency of 50π rad/s is selected because it corresponds to 500 r/min rotor speed and the accuracy of the voltage model based observer is satisfactory above this speed. The Ψ_{main} is generated from a predefined look-up table.

TABLE I
IPMSM PARAMETERS

Number of pole-pairs	3
Phase resistance	51.2 m Ω
Continuous/Maximum current	58.5/118 A
Peak power at base speed	10 kW
DC link voltage	120 V
Base/maximum speed	1350/4500 r/min
Continuous/peak torque	35.5/70 N·m
Peak power at maximum speed	7 kW

The influences of the flux observer accuracy on direct flux vector control and the effectiveness of the reference flux amplitude compensation term, $\Delta\Psi_s$, are studied by simulation when the drive operates in the constant torque region with 45 N·m reference torque at 1000 r/min. A high fidelity IPMSM model with due account of temperature effects on phase resistance and permanent magnet flux linkage is employed to represent more realistic machine behavior in the simulation. Variations of the PM flux linkage and the d- and q-axis inductances, at nominal operating temperature of 20 °C, with currents are mapped in the flux observer and the inverter is assumed to be ideal. Thus, the observer will be accurate in steady-state if the phase resistance, d- and q-axis inductances and the PM flux linkage used in the observer are the same as those in the machine model. However, observer errors can be deliberately injected in the simulations.

Fig. 5 shows simulation results when the observed flux amplitude, $\hat{\Psi}_s$, and the observed angle between the f-axis and d-axis, $\hat{\delta}$, are accurate, when $\hat{\Psi}_s$ is 10% lower but $\hat{\delta}$ is accurate, and when $\hat{\Psi}_s$ is accurate but $\hat{\delta}$ is 10% lower. The MTPA points tracked by the proposed control scheme are denoted by the triangles and the control results of the DFVC without $\Delta\Psi_s$ are denoted by the squares. The corresponding constant current amplitude loci with the ideal MTPA points marked by the circles are also illustrated in Fig. 5. As can be seen, when the flux observer is accurate, both control schemes operate at the MTPA point and the output torque equals to the reference torque. Torque control errors occur when the observed flux deviates. For example, when $\hat{\Psi}_s$ is 10% lower, the resultant torque is greater than the reference of 45 N·m because the reference flux t-axis current generated by (6) is greater than what is required. On the other hand when $\hat{\delta}$ is 10% lower, the magnitude of the t-axis current is correct, but its angle is inaccurate. Consequently, the net torque production component is reduced and hence the resultant torque is lower than the reference. However, the proposed control scheme is still capable of tracking the reference flux amplitudes to the actual MTPA flux amplitude despite of large torque errors. In contrast, the observer magnitude error cause a significant deviation from the MTPA point with the direct flux vector control without flux amplitude compensation, which will increase copper loss.

It should be noted that torque control error is inevitable when the observed flux vector is not accurate. However, the torque

error can be corrected by the speed feedback loop in a speed servo drive. For EV tractions, the feedback correction will be performed by a human driver.

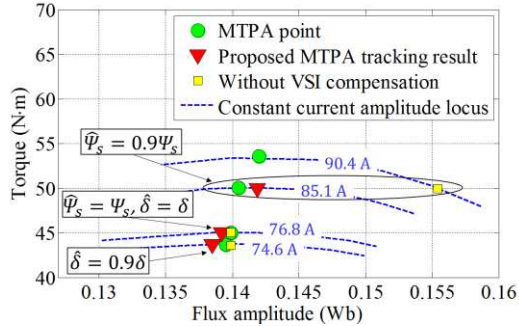


Fig. 5. Influence of the observed flux amplitude error and angle error on MTPA tracking of proposed control scheme and DFVC without VIS.

The temperature influence on the proposed control scheme has also been studied by employing a temperature dependent machine model. From the design data of the prototype machine, the stator resistance increases 39% per 100 °C temperature rise and the remanence of the permanent magnets decreases 12% per 100 °C temperature rise. However, machine parameters in flux observer and the model for generating Ψ_{main} assumes a constant temperature of 20 °C. The influence of temperature on MTPA point tracking performance of the proposed control scheme is simulated. The simulation result is shown in Fig. 6 where the stator temperature in the machine model is changed from 20 °C to 120 °C at $t=15$ s. Due to the machine parameter variations with temperature, the flux observer is no longer accurate. Consequently, the torque and the optimal flux amplitude decrease when the temperature is increased. However, Ψ_s^* which is generated by the proposed control follows the optimal MTPA flux amplitude of the new machine parameters closely. It follows from the simulation results shown in Fig. 5 and Fig. 6 that the proposed control scheme is robust to flux observer errors in tracking MTPA points.

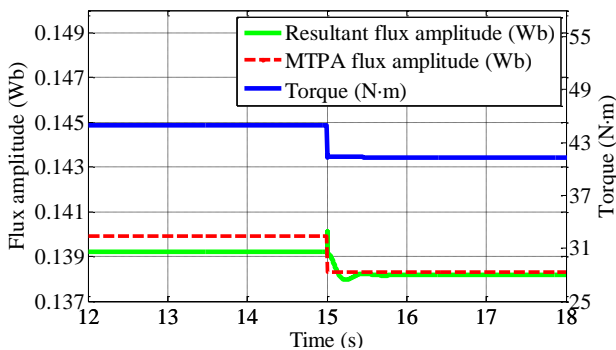


Fig. 6. MTPA point tracking performance when temperature changes at 1000 r/min.

V. EXPERIMENTAL RESULT

The proposed direct flux vector control scheme has been tested on the prototype IPMSM drive. The motor whose specifications are given in Table I is mounted on the experimental test-rig as shown in Fig. 7. During the tests, the motor was loaded by a dynamometer and controlled in torque

control mode. The torque was measured by a high precision torque transducer. The frequency and amplitude of the virtual signal was 1000 Hz and 0.001 rad, respectively. A 4th order band-pass filter with 1 Hz band width at the center frequency was employed. The L_d, L_q, Ψ_m in the current model of the flux observer are set to their nominal values, i.e., 0.64 mH, 1.84 mH and 0.1132 Wb, respectively. ξ and ω_0 in Fig. 4 are set to 0.707 and 50π rad/s, respectively. The Ψ_{main} is generated from a predefined look-up table.

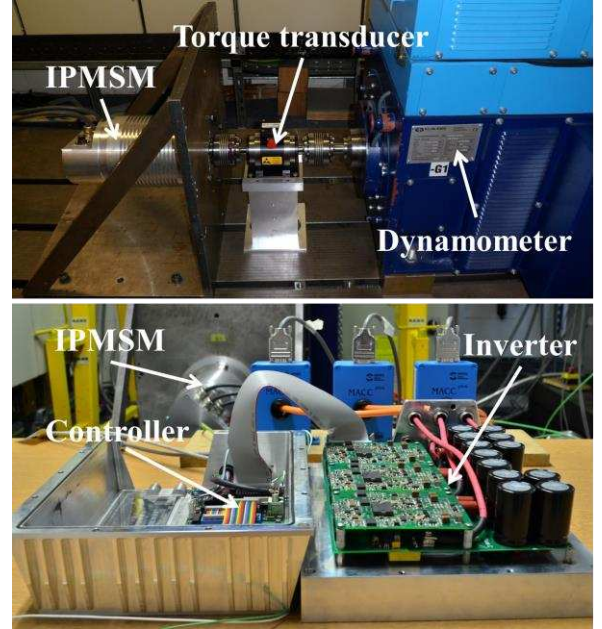


Fig. 7. Experimental test-rig.

A. Validation of machine parameters independent MTPA control

For the conventional look-up table based direct flux vector control [8], i.e., Part I in Fig. 3, the accuracy of MTPA operation is highly depend on Ψ_{main} and the accuracy of flux observer. However, the proposed virtual signal injection based direct flux vector control can automatically and accurately track the MTPA points without knowing machine parameters except for the nominal machine parameters in flux observer expressed in (24).

In order to verify the MTPA tracking performance of the proposed control scheme, experiments were first performed by setting Ψ_{main} as a constant value, i.e., $\Psi_{main} = 0.1$ Wb. The drive was tested at 1000 r/min and torque varied from 5 N·m to 35 N·m. Since the actual flux amplitude is difficult to measure, the measured d-axis current is utilized instead of flux amplitude to illustrate the MTPA tracking performance of the proposed control scheme. As shown in Fig. 8, the drive is enabled with 5 N·m reference torque at time=4 s. At beginning, due to the inaccurate Ψ_{main} , the resultant d-axis current is quite large, about -30 A. However, $\Delta\Psi_s$ in Fig. 3 automatically compensates the error of reference flux amplitude until the MTPA point is reached. Moreover, as shown in Fig. 8, for each torque step, the proposed control scheme always tracks the MTPA points accurately although a small overshoot can be observed in the measured d-axis current. The response of the

proposed control scheme can be improved by a more accurate Ψ_{main} .

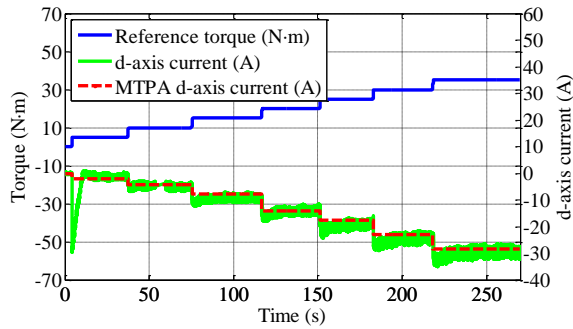


Fig. 8. Measured d-axis current, MTPA d-axis current, and reference torque.

Fig. 9 shows the variation of d-axis current with the output of LPF 1 which is utilized to generate $\Delta\Psi_s$. As shown in Fig. 9, at each torque step, the output of LPF 1 is initially large then decrease to zero, which indicates that the MTPA point is tracked gradually, until $-\partial T_e/\partial\beta = 0$.

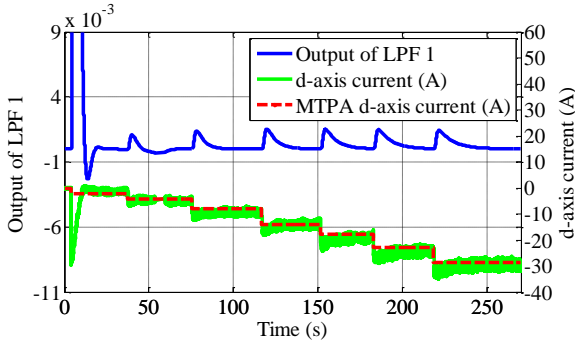


Fig. 9. The output of LPF 1 and measured d-axis current.

B. Independence of flux observer error in MTPA operation

Since $\Delta\Psi_s$ is based on measured currents in the d-q frame, the flux observer error does not affect the MTPA tracking performance of the proposed control scheme. In order to verify the independence of flux observer error, the proposed control scheme and the conventional DFVC without $\Delta\Psi_s$ were tested at 400 r/min when the reference torque was stepped from 0 N·m to 5 N·m. The Ψ_{main} in both control schemes were generated by the same pre-defined look-up table which was obtained from a high fidelity nonlinear IPMSM machine model [24]. The high fidelity IPMSM machine model was generated from numerical analysis of electromagnetic field based on finite element analysis.

Because of inverter nonlinearity and voltage drop, the flux observer illustrated in Fig. 4 may have large error at low reference torque and low speed, i.e., low current amplitude and low voltage amplitude. The comparison between proposed control scheme and the DFVC without $\Delta\Psi_s$ is shown in Fig. 10. As can be seen, when the reference torque is 0 N·m, the resultant d-axis current of the proposed control scheme is 0 A, being the same as the MTPA d-axis current. However, the resultant d-axis current of the DFVC without $\Delta\Psi_s$ is about 10 A which is caused by the errors in both the flux observer and

Ψ_{main} . This will lead to large copper loss and inefficient operation.

When reference torque steps to 5 N·m, the resultant d-axis current of the proposed control scheme follows the MTPA d-axis current accurately, however, the error between the MTPA d-axis current and the resultant d-axis current of the conventional DFVC without $\Delta\Psi_s$ remains large. The high MTPA tracking accuracy of the proposed control scheme is due to the fact that $\Delta\Psi_s$ in Fig. 3 automatically compensates the errors in both Ψ_{main} and flux observer.

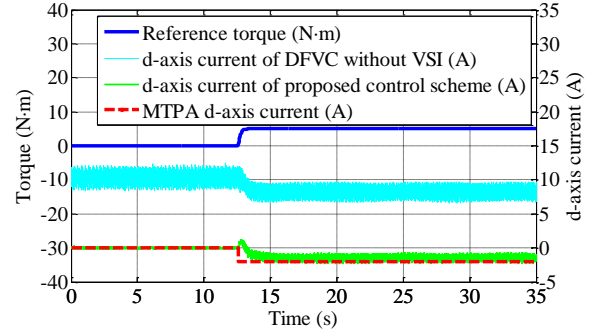


Fig. 10. Comparison between proposed control scheme and conventional control scheme at 400r/min when reference torque steps from 0N·m to 5N·m.

The MTPA tracking performance of the proposed control scheme was also tested at various speeds and reference torques in steady state. Fig. 11 and Fig. 12 show the MTPA control performances of the proposed control scheme and the DFVC without $\Delta\Psi_s$ when the motor drive operates at 400 r/min and 1000 r/min, respectively. At both speeds, the motor drive was tested by varying the reference torque from 10 N·m to 35 N·m in steps of 5 N·m. Again, the Ψ_{main} in both control schemes were generated by the same pre-defined look-up table as described previously. The MTPA tracking results of the proposed control scheme are denoted by triangles in Fig. 11 and Fig. 12, whereas the control results of the DFVC without $\Delta\Psi_s$ are denoted by squares. Tests were also performed by varying the current vector angle while its magnitude was kept constant. The results are shown in the curve marked by the crosses. The exact MTPA points, denoted by the circles, can be obtained by using curve-fitting of the constant current amplitude loci for the different reference torques.

Comparing Fig. 11 with Fig. 12, it can be seen that the MTPA tracking errors of the DFVC without $\Delta\Psi_s$ are dependent on both torque and speed. Since Ψ_{main} generated from the look-up table for a given reference torque in constant torque region is independent of speed, the deviations of the control results must be caused by observer errors. However, although the Ψ_{main} and flux observer in the proposed control scheme are the same as those in the DFVC without $\Delta\Psi_s$ under test, the proposed control scheme can track the MTPA points accurately and consistently. Therefore, the flux observer independence of the proposed control scheme in tracking MTPA points can be verified.

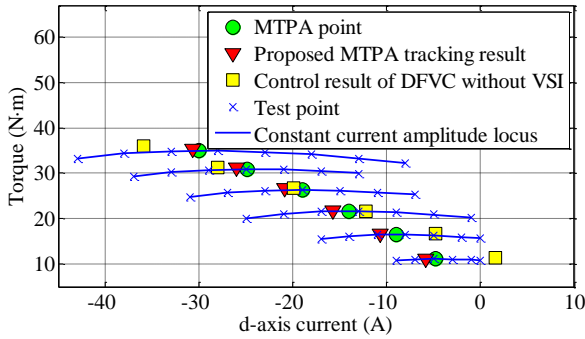


Fig. 11. Comparison of MTPA tracking performance of proposed control scheme and conventional DFVC at 400 r/min.

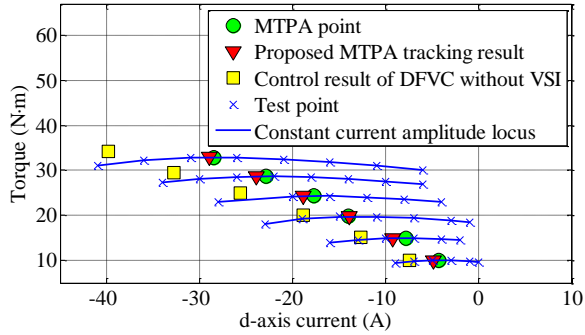


Fig. 12. Comparison of MTPA tracking performance of proposed control scheme and conventional DFVC at 1000 r/min.

To illustrate the quality of MTPA tracking of the proposed control scheme, the experiment results of torque per current at 1000 r/min obtained from the proposed and conventional DFVC without $\Delta\psi_s$ are compared with the MTPA points in Fig. 13. Again, the good MTPA tracking of the proposed control scheme can be observed. It is worth noting that since the MTPA points are obtained from curve-fitting of the measured constant current amplitude loci and the machine parameters varies with temperature during the measurement, the MTPA points in Fig. 13 may contain small errors.

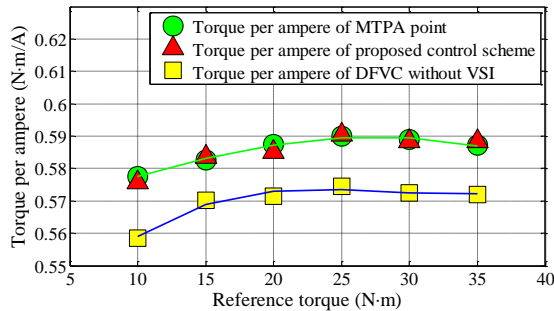


Fig. 13. Comparison of torque per ampere variations of proposed and conventional control schemes at 1000 r/min.

Since the MTPA tracking performance of the DFVC without VSI is mainly dependent on the accuracy of ψ_{main} and $\hat{\varphi}_s$. An inaccurate ψ_{main} and $\hat{\varphi}_s$ may cause large deviation from the MTPA point as shown in Fig. 8 at $t=4$ s. Hence, due to the nonlinearity and uncertainty of machine parameters, the MTPA control performance of the DFVC without VSI is difficult to guarantee. However, the MTPA control accuracy can always be guaranteed by the proposed control scheme.

C. Performance of proposed control scheme during payload torque change

The MTPA tracking performance of the proposed control scheme during payload torque changes is shown in Fig. 14. The motor was operated at 1000 r/min and a step change in reference torque from 30 N·m to 35 N·m was applied. The dashed line represents the actual MTPA d-axis currents at 30 N·m and 35 N·m at 1000 r/min. It can be seen that the corresponding d-axis currents generated by the proposed control scheme are very close to the actual MTPA d-axis currents during the torque step change.

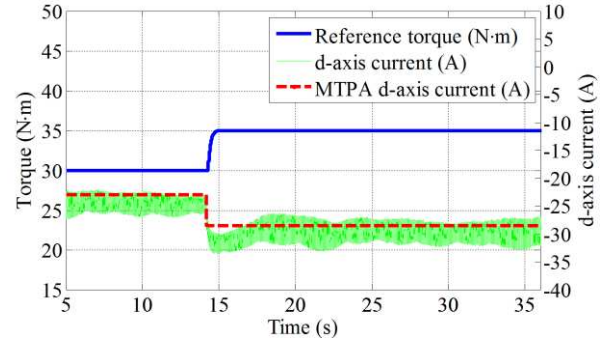


Fig. 14. MTPA tracking response of proposed control scheme to step change in reference torque at speed of 1000 r/min.

Fig. 15 shows the response of LPF 1 to the step change in reference torque. The output of LPF 1 is proportional to $\partial T_e / \partial \beta$. As can be seen, the torque change results in deviation from the MTPA operation, and consequently, $\partial T_e / \partial \beta$ is no longer zero but it is used to adjust the flux amplitude reference until $\partial T_e / \partial \beta$ becomes zero again, i.e., reaching the new MTPA point.

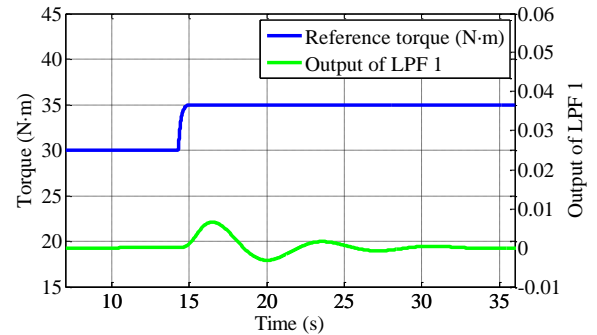


Fig. 15. Response of LPF 1 to torque step change at 1000 r/min.

Fig. 16 shows the measured and estimated torque responses to a step change in reference torque. The estimated torque is calculated from the machine parameters stored in look-up tables with the measured d- and q-axis current. It can be seen that the torque responds fast and the small error between the reference and measurement may be caused by the combined effect of the observer error and friction torque which is not accounted in the torque reference.

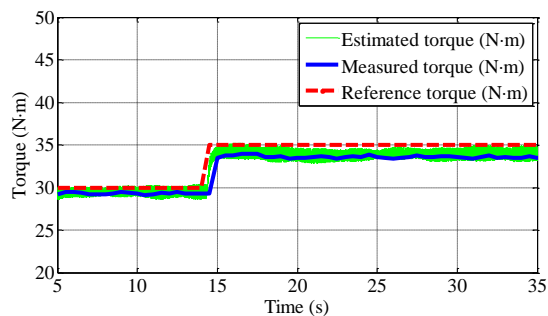


Fig. 16. Measured torque and torque reference at 1000 r/min.

D. Performance of proposed control scheme at low speed

In order to verify the performance of the proposed control scheme at low speeds when the d- and q-axis voltages are small, the motor drive was tested at 15 r/min. Fig. 17 shows the estimated/measured torque and measured d-axis current responses when the reference torque steps from 15 N·m to 20 N·m. Again the dash line in Fig. 17 indicates the actual MTPA d-axis currents associated with 15 N·m and 20 N·m at 15 r/min. It can be seen that the proposed control scheme can still track the MTPA point accurately although the torque error is noticeable. In order to avoid dividing by zero at very low speeds when processing the right hand side of (20), the $\Delta\Psi_s$ term can be suspended when the measured speed is below a minimum threshold.

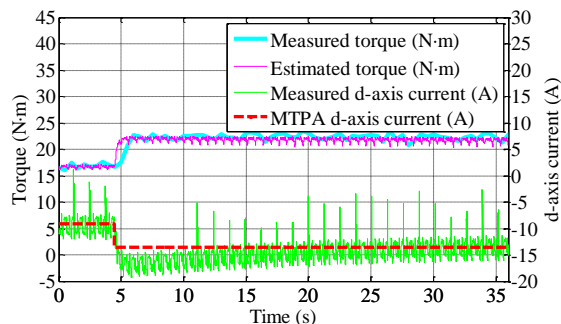


Fig. 17. MTPA tracking response of proposed control scheme to step change in reference torque at 15 r/min.

VI. CONCLUSION

The proposed virtual signal injection based direct flux vector control scheme provides a parameter independent and observer error insensitive method to achieve accurate MTPA control of IPMSM drives in constant torque region. Because high frequency signal is injected virtually, the proposed method does not cause any additional iron/copper loss and is very robust to voltage and current harmonics. The proposed method also avoids any torque or speed ripple and resonant problems caused by current ripple associated with real signal injection. Because the signal injection is based on d- and q-axis quantities, the proposed control scheme is not affected by the observer's error in tracking MTPA operation. Both simulation results and experiment results demonstrate that the proposed method can track the MTPA points in constant torque region accurately and automatically.

REFERENCES

- [1] M. Koc, J. Wang, and T. Sun, "An Inverter Nonlinearity Independent Flux Observer for Direct Torque Controlled High Performance Interior Permanent Magnet Brushless AC Drives," *IEEE Trans. Power Electron.*, DOI 10.1109/TPEL.2016.2524644, in press, 2016.
- [2] X. Liu, H. Chen, J. Zhao, and A. Belahcen, "Research on the Performances and Parameters of Interior PMSM Used for Electric Vehicles," *IEEE Trans. Ind. Electron.*, DOI 10.1109/TIE.2016.2524415, in press, 2016.
- [3] Y. Ren and Z. Q. Zhu, "Enhancement of Steady-State Performance in Direct Torque Controlled Dual-three Phase Permanent Magnet Synchronous Machine Drives with Modified Switching Table," *IEEE Trans. Ind. Electron.*, vol. 62, DOI 10.1109/TIE.2014.2376881, no. 6, pp. 3338–3350, Jun. 2015.
- [4] J. S. Lee and R. D. Lorenz, "Robustness Analysis of Deadbeat-Direct Torque and Flux Control for IPMSM Drives," *IEEE Trans. Ind. Electron.*, DOI 10.1109/TIE.2016.2521353, in press, 2016.
- [5] C. Xia, S. Wang, X. Gu, Y. Yan, and T. Shi, "Direct Torque Control for VSI-PMSM Using Vector Evaluation Factor Table," *IEEE Trans. Ind. Electron.*, DOI 10.1109/TIE.2016.2535958, in press, 2016.
- [6] Y.-S. Choi, H. H. Choi, and J.-W. Jung, "Feedback Linearization Direct Torque Control with Reduced Torque and Flux Ripples for IPMSM Drives," *IEEE Trans. Power Electron.*, vol. 31, DOI 10.1109/TPEL.2015.2460249, no. 5, pp. 3728–3737, May. 2016.
- [7] G. Pellegrino, E. Armando, and P. Guglielmi, "Direct Flux Field-Oriented Control of IPM Drives With Variable DC Link in the Field-Weakening Region," *IEEE Trans. Ind. Appl.*, vol. 45, DOI 10.1109/TIA.2009.2027167, no. 5, pp. 1619–1627, Sept./Oct. 2009.
- [8] G. Pellegrino, E. Armando, and P. Guglielmi, "Direct-Flux Vector Control of IPM Motor Drives in the Maximum Torque Per Voltage Speed Range," *IEEE Trans. Ind. Electron.*, vol. 59, DOI 10.1109/TIA.2009.2027167, no. 10, pp. 3780–3788, Oct. 2012.
- [9] G. Pellegrino, R. I. Bojoi, and P. Guglielmi, "Unified Direct-Flux Vector Control for AC Motor Drives," *IEEE Trans. Ind. Appl.*, vol. 47, DOI 10.1109/TIA.2011.2161532, no. 5, pp. 2093–2102, Sept./Oct. 2011.
- [10] G. Pellegrino, E. Armando, and P. Guglielmi, "Direct-flux field-oriented control of IPM motor drives with robust exploitation of the Maximum Torque per Voltage speed range," in *Proc. IEEE ISIE*, DOI 10.1109/ISIE.2010.5637031, Jul. 2010, pp. 1271–1277.
- [11] X. Xu and D. W. Novotny, "Selection of the flux reference for induction machine drives in the field weakening region," *IEEE Trans. Ind. Appl.*, vol. 28, DOI 10.1109/28.175288, no. 6, pp. 1353–1358, Nov./Dec. 1992.
- [12] C. Xia, J. Zhao, Y. Yan, and T. Shi, "A Novel Direct Torque Control of Matrix Converter-Fed PMSM Drives Using Duty Cycle Control for Torque Ripple Reduction," *IEEE Trans. Ind. Electron.*, vol. 61, DOI 10.1109/TIE.2013.2276039, no. 6, pp. 2700–2713, Jun. 2014.
- [13] T. Inoue, Y. Inoue, S. Morimoto, and M. Sanada, "Mathematical Model for MTPA Control of Permanent-Magnet Synchronous Motor in Stator Flux Linkage Synchronous Frame," *IEEE Trans. Ind. Appl.*, vol. 51, DOI 10.1109/TIA.2015.2417128, no. 5, pp. 3620–3628, Sept./Oct. 2015.
- [14] D. Q. Dang, M. S. Rafiq, H. H. Choi, and J.-W. Jung, "Online Parameter Estimation Technique for Adaptive Control Applications of Interior PM Synchronous Motor Drives," *IEEE Trans. Ind. Electron.*, vol. 63, DOI 10.1109/TIE.2015.2494534, no. 3, pp. 1438–1449, Mar. 2016.
- [15] Y. Tan, W. H. Moase, C. Manzie, D. Nešić, and I. M. Mareels, "Extremum Seeking From 1922 To 2010," in *Proc. IEEE CCC*, Jul. 2010, pp. 14–26.
- [16] R. Antonello, M. Carraro, and M. Zigliotto, "Maximum-Torque-Per-Ampere Operation of Anisotropic Synchronous Permanent-Magnet Motors Based on Extremum Seeking Control," *IEEE Trans. Ind. Electron.*, vol. 61, DOI 10.1109/TIE.2013.2278518, no. 9, pp. 5086–5093, Sept. 2014.
- [17] S. Kim, Y. D. Yoon, S. K. Sul, and K. Ide, "Maximum Torque per Ampere (MTPA) Control of an IPM Machine Based on Signal Injection Considering Inductance Saturation," *IEEE Trans. Power Electron.*, vol. 28, DOI 10.1109/TPEL.2012.2195203, no. 1, pp. 488–497, Jan. 2013.
- [18] S. Bolognani, L. Peretti, and M. Zigliotto, "Online MTPA Control Strategy for DTC Synchronous-Reluctance-Motor Drives," *IEEE Trans. Power Electron.*, vol. 26, DOI 10.1109/TPEL.2010.2050493, no. 1, pp. 20–28, Jan. 2011.
- [19] T. Sun, J. Wang, and X. Chen, "Maximum Torque per Ampere (MTPA) Control for Interior Permanent Magnet Synchronous Machine Drives Based on Virtual Signal Injection," *IEEE Trans. Power Electron.*, vol. 30, DOI 10.1109/TPEL.2014.2365814, no. 9, pp. 5036–5045, Sept. 2015.

- [20] T. Sun, J. Wang, M. Koc, and X. Chen, "Self-Learning MTPA Control of Interior Permanent Magnet Synchronous Machine Drives Based on Virtual Signal Injection," *IEEE Trans. Ind. Appl.*, DOI 10.1109/TIA.2016.2533601, in press, 2016.
- [21] T. Sun and J. Wang, "Extension of Virtual Signal Injection Based MTPA Control for Interior Permanent Magnet Synchronous Machine Drives into Field Weakening Region," *IEEE Trans. Ind. Electron.*, vol. 62, DOI 10.1109/TIE.2015.2438772, no. 11, pp. 6809–6817, Nov. 2015.
- [22] G. Pellegrino, B. Boazzo, and T. M. Jahns, "Direct Flux Control of PM Synchronous Motor Drives for Traction Applications," in *Proc. IEEE ITC*, DOI 10.1109/ITC.2014.6861836, Jun. 2014, pp. 1–6.
- [23] J.-W. Choi and S.-K. Sul, "Inverter output voltage synthesis using novel dead time compensation," *IEEE Trans. Power Electron.*, vol. 11, DOI 10.1109/63.486169, no. 2, pp. 221–227, Mar. 1996.
- [24] X. Chen, J. Wang, B. Sen, P. Lazari, and T. Sun, "A High-Fidelity, Computationally Efficient Model for Interior Permanent Magnet Machines Considering the Magnetic Saturation, Spatial Harmonics and Iron Loss Effect," *IEEE Trans. Ind. Electron.*, vol. 62, DOI 10.1109/TIE.2014.2388200, no. 7, pp. 4044–4055, Jul. 2015.
- [25] A. Yoo and S. K. Sul, "Design of Flux Observer Robust to Interior Permanent-Magnet Synchronous Motor Flux Variation," *IEEE Trans. Ind. Appl.*, vol. 45, DOI 10.1109/TIA.2009.2027516, no. 5, pp. 1670–1677, Sept./Oct. 2009.



Tianfu Sun (S'15) was born in China. He received B.Eng. degree in mechanical engineering and M.Sc. degree in civil engineering from Dalian University of Technology, Dalian, China, in 2009 and 2012, respectively.

He is currently pursuing the Ph.D. degree in electronic and electrical engineering at The University of Sheffield, U.K. His current research interests include electric/hybrid

vehicle drives, power-electronic control of electric machines, sensorless drives and artificial intelligence.



Jiabin Wang (SM'03) received the B.Eng. and M.Eng. degrees from Jiangsu University of Science and Technology, Zhenjiang, China, in 1982 and 1986, respectively, and the Ph.D. degree from the University of East London, London, U.K., in 1996, all in electrical and electronic engineering.

Currently, he is a Professor in Electrical Engineering at the University of Sheffield, Sheffield, U.K. From 1986 to 1991, he was with the Department of Electrical Engineering

at Jiangsu University of Science and Technology, where he was appointed a Lecturer in 1987 and an Associated Professor in 1990. He was a Postdoctoral Research Associate at the University of Sheffield, Sheffield, U.K., from 1996 to 1997, and a Senior Lecturer at the University of East London from 1998 to 2001. His research interests range from motion control and electromechanical energy conversion to electric drives for applications in automotive, renewable energy, household appliances and aerospace sectors.

He is a fellow of the IET and a senior member of IEEE.



Mikail Koc (S'15) was born in Turkey. He received the BSc degree from ESOGU University, Eskisehir, Turkey, in 2009 and the MSc degree from Nottingham University, UK, in 2012 both in electrical and electronic engineering. He is currently pursuing the PhD degree in electronic and electrical engineering at the University of Sheffield, UK. His research interests include efficiency optimised control of motors for electric vehicle

traction.